DALTON

# Defect fluorite-type structures: modelling triclinic lanthanoid oxides*

**Raymond L. Martin**

*School of Chemistry, Monash University, Clayton, Victoria 3168, Australia*

The co-ordination defect (c.d.) theory of fluorite-related structures has been compared and contrasted with the recently published phenomenological modular model. It is confirmed that the integrity and topology of the co-ordinated defect play a pivotal role in determining the structures of the higher lanthanoid oxides and that the c.d. diagrams derived from topological analysis enable both known and unknown model structures to be predicted. The predictive limitations of the phenomenological modular model are exposed and it is shown that fluorite modular sequences derived therefrom are already encapsulated in the $\{100\}_F$ c.d. diagrams for the $M_nO_{2n-2}$ oxide phases. A new set of modules is proposed that is not only compositionally identical to that previously reported but which also possesses the cardinal advantage of incorporating the structure-determining topology of the co-ordination defect.

The binary oxides of lanthanoid (or rare earth) elements that exhibit higher oxidation states (M = Ce, Pr or Tb) are characterized at higher temperatures by non-stoichiometric phases of extended compositional width. Prolonged annealing at lower temperatures resolves these phases into a homologous series of discrete ordered intermediate oxides of well defined composition which are expected to be interrelated by some common structural principle. It is now well established that these phases are oxygen deficient with respect to the parent dioxide $MO_2$, they are fluorite related, and their compositions conform to the homologous series $M_nO_{2n-2m}$ (see Table 1).

Structural characterization of these binary refractory oxides has proved to be a long term and on-going challenge. The synthesis of well ordered crystals is inherently difficult due to the high mobility of oxygen in the lattice. Although very small crystals have been grown by hydrothermal techniques, problems associated with crystallographic twinning, coherent intergrowth between the phases, absorption errors and large superstructures of low symmetry have all combined to make definitive determinations of structure a formidable task.

For more than four decades[2,3] the exact way by which gross concentrations (*i.e.* up to 25%) of vacant oxygen sites could be accommodated in the fluorite $MO_2$ lattice remained unresolved although informative indications were contained in early X-ray powder diffraction data for the ternary $M_7O_{12}$ phases $UY_6O_{12}$ and $Zr_3Sc_4O_{12}$.[4] Clearly there was a pressing need for a theory which, in the absence of crystallographic data, would enable structural models to be predicted for each member of the homologous series and their polymorphs. Further, if the structural principle that underlies the ordering of vacant anion sites were identified, the homology which characterizes these intermediate oxides would be better understood.

It was against this background that in 1974 a theory of defect fluorite-type structures was put forward[5] which enabled model structures to be predicted for individual members of the extended $M_nO_{2n-2}$ series of lanthanoid oxides. The central core of this theory was the idea that a vacant anion site, □, would have no independent existence in the fluorite lattice but would be strongly co-ordinated by its six nearest $O^{2-}$ neighbours to form an octahedral structural entity, $□O_6$, of considerable thermodynamic stability. Since the face-centred cubic cation lattice was known to remain intact in these phases, the total composition of the co-ordinated defect (or c.d.) was formulated as $M_{3.5}□O_6$. This description of the local environment of vacant oxygen sites in fluorite-type structures is now acknowledged to be correct.[6,7]

**Table 1** Some binary triclinic lanthanoid oxides

| O : M | $M_nO_{2n-2m}$ | M(*m*) | Modular sequence along $[001]_F$ [a] |
|---|---|---|---|
| 1.714 | ι-$M_7O_{12}$ | Ce, Pr, Tb (1) | $[H^1L_1H^2W_2^4L_4H^3L_3]$ |
| 1.750 | $M_8O_{14}$ | Unknown | $[H^1H^4L_4H^3L_1H^2L_2L_3]$ |
| 1.778 | ζ-$M_9O_{16}$ | Pr (1) | $[FL_2H^3H^1H^2L_4L_3L_1H^4]$ [b] |
| 1.789 | $M_{19}O_{34}$ | Ce (2) | $[3F8H^i8L_j]$ or $[4FW_j^i7H^i7L_j]$ [c] |
| 1.818 | δ-$M_{11}O_{20}$ | Ce, Tb (1) | $[FL_3L_4H^3H^4FFL_2L_1H^2H^1]$ |

[a] See Table 2 and **Conclusion**. [b] Along $[011]_F$. [c] Modular cell content.

This 'co-ordination defect' or c.d. model[5] was further developed by employing an oxygen-centred representation of the fluorite cube with the primitive octant, $M_{1/2}O$, being used as the fundamental building block or module on which the $M_nO_{2n-2m}$ superstructures were based. Central elements of this theory were the recognition that (i) the tetrahedron of metal atoms located on each $M_{1/2}O$ octant would possess either a right- or left-handed orientation and (ii) there would be well defined topological restrictions on the number of ways that a c.d. (*i.e.* a co-ordinated vacant site) could be deployed in the fluorite lattice. In 1974, because of the absence of detailed knowledge of the symmetry and dimensions of the unit cells of the intermediate lanthanoid oxides, application of the theory was necessarily limited to the development of plausible but not proven structural models for all binary oxides in the composition range $M_2O_3$ to $MO_2$.

In 1975 Kunzmann and Eyring[8] succeeded in determining the symmetry and unit-cell dimensions for each of the homologues with $n = 7$, 9, 10, 11 and 12 from electron diffraction patterns taken with a high-resolution transmission electron microscope using very small crystals. Evaluation of the c.d. theory in the light of these new data confirmed that the structural principles on which it was based were correct and enabled Hoskins and Martin[9] in 1976 to predict all of the possible structures for each of the odd homologues with $n = 7$, 9 and 11. Thus for the oxides $M_7O_{12}$, $M_9O_{16}$ and $M_{11}O_{20}$ application of the theory confirmed that there were only one, two and three models, respectively, which were consistent with the published unit-cell parameters. The main structural features of each model were described.[9]

At that time the even-numbered homologues ε-$M_{10}O_{18}$ and β-$M_{12}O_{22}$ were more difficult to model in part because of their large supercells and in part because Kunzmann and Eyring

* A structural theory for non-stoichiometry. Part 6.[1]

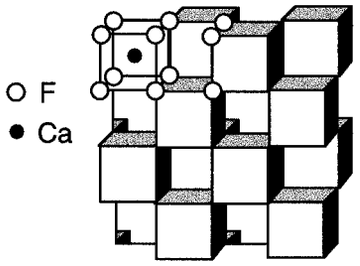


**Fig. 1** Fluorite structure represented as an array of edge-sharing $MO_8$ cubes

overlooked the presence of a $2_1$ screw axis which led them to an incorrect assignment of the space group as *Pn* rather than $P2_1/c$. Even so, application of the c.d. model using the incorrect space group illuminated the broad features to be expected for these monoclinic phases.[9]

Now two decades later it has become possible to elucidate the structures of powdered solids from high-resolution time-of-flight neutron diffraction data. In this the experimentally observed neutron diffraction profile is compared to the profile calculated for a trial model of the structure. A valuable feature of the c.d. theory is that it provides a useful tool for both devising and minimizing the number of trial structures required for comparison of calculated and observed diffraction data.

Using this technique Eyring and co-workers[10–13] have put forward structures for the oxygen-deficient $M_nO_{2n-2}$ homologues with $n = 7$, 9, 10, 11 and 12 (arbitrarily taking $m = 1$) and depicted these in terms of the $M_4$ metal tetrahedra which circumscribe the oxygen vacancies with the viewing direction projected along $\frac{1}{2}[21\bar{1}]_F$. Hoskins and Martin[1] have shown that the proposed new structures confirm that the intricate patterns of planar ordering of anion vacancies found in the defect fluorite lattice arise from the unique and structure-determining topology of the co-ordination defect. Further, they have formulated a hierarchy which interrelates all the binary fluorite-related oxides in the composition range $M_2O_3$ to $M_2O_4$.

The determination of these five structures has encouraged Eyring and his co-workers[6,14] to propose a new 'phenomenological structural principle' with which they claim to be able to model all known structures correctly as well as to model any unknown structure in the series providing the composition and lattice parameters of the supercells are known. Owing to the central position played by this extended series of fluorite-type defect oxides in the current theory of non-stoichiometric oxides, it is important to evaluate and establish the status of the two competing theories in this area of solid-state chemistry. In this paper the recent 'structural principle' of Eyring and co-workers will be compared and contrasted with the earlier[5] co-ordination defect model. It will emerge that, while there is necessarily a considerable degree of congruence between the old and the new approaches, there are inherent limitations in the new approach.

## The Fluorite Structure

The dioxides of the quadrivalent lanthanoid elements adopt the crystal structure of fluorite, $CaF_2$. The $M^{4+}$ cations are in a face centred cubic (f.c.c.) array which interpenetrates with a simple cubic lattice of $O^{2-}$ anions. Each cation is eight-co-ordinated and lies at the centre of a cube of anions. The composition $MO_2$ is achieved by face sharing of $MO_8$ cubes with an equal number of $O_8$ cubes from which the cation is missing (see Fig. 1). The unit cell comprises four $MO_8$ and four $O_8$ cubes with the overall composition $M_4O_8$.

In the anion-deficient lanthanoid oxides, $M_nO_{2n-2}$, the non-stoichiometry is centred on untenanted anion sites. The cation lattice remains fully occupied and f.c.c. albeit with small but significant distortions in the vicinity of the vacant sites.

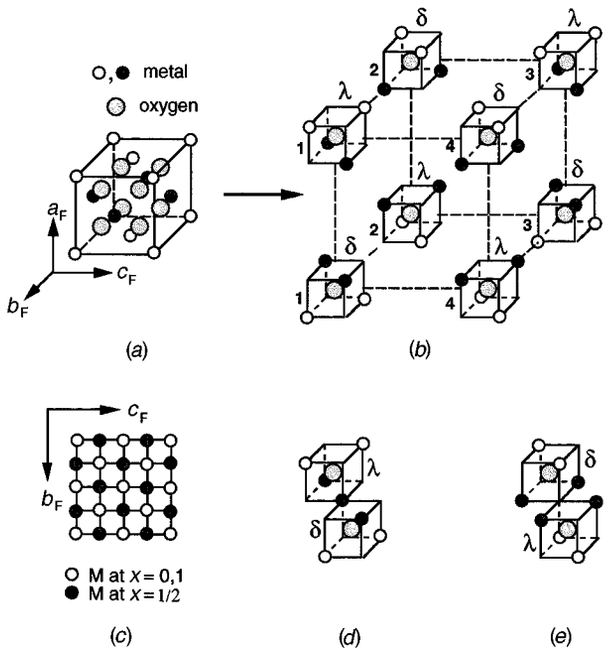


**Fig. 2** Fluorite structure. (*a*) Unit cell of composition $M_4O_8$. (*b*) Unit cell exploded into eight octants, four with δ and four with λ phasing of the metal atoms. (*c*) Matrix representation for a $\{100\}_F$ layer of 16 octants (composition $M_8O_{16}$). (*d*) Metal-centred (δ, λ) octant pair with O–M–O oriented along the $[1\bar{1}\bar{1}]_F$ direction. (*e*) Corner-sharing (λ, δ) octant pair

Attempts to represent the superstructure patterns of ordered defects in terms of metal-centred polyhedra such as $MO_8$, $MO_7$ $MO_6$ and metal-free $O_8$, $O_7$, $O_6$ polyhedra prove to be somewhat cumbersome and provide only a limited insight into the planar distribution of vacant sites found[1] in oxides which deviate from the parent $MO_2$ composition.

In order to circumvent this problem the author[5] devised an alternative and more informative representation of vacant sites in the fluorite anion lattice by changing the frame of reference from metal-centred to anion-centred polyhedra. The unit cell of $MO_2$ [see Fig. 2(*a*)] can then be contemplated in alternative terms as an assembly of eight octants of the fluorite cube, each with an oxide anion at its centre. Four $M^{4+}$ cations are tetrahedrally disposed about each oxygen and lie at the alternating corners of the octant cube [see Fig. 2(*b*)]. Each octant of composition $M_{4/8}O$ and dimension $\frac{1}{2}a$ shares all its faces with nearest octant neighbours to generate the fluorite lattice in three dimensions [see Fig. 2(*a*)]. A two-dimensional layer of octants can be represented by the square matrix illustrated in Fig. 2(*c*). The f.c.c. array of metal atoms is arranged at appropriate intersections of the matrix whereas the oxygen atoms in projection are situated at the centre of each square. Thus for the reference $(100)_F$ octant layer the cation origins would be at $x = 0$ and $\frac{1}{2}$ with the anions at $x = \frac{1}{4}$. It is convenient here to introduce a new co-ordinate $X$ to designate the height of the centre of a particular layer of octants above the reference plane at $X = 0$; for example, an $X = 1$ layer would refer to the layer of $(100)_F$ octants which are centred on oxide anions with $x = \frac{3}{4}$, the cations being located at $x = \frac{1}{2}$ and 1. Kang and Eyring[6] in their new approach have followed this oxygen-centred perspective by regarding the fluorite lattice as comprised of tetrahedrally co-ordinated oxygen atoms which they write as '$(R_4O)$'.

It is evident from Fig. 2(*b*) that the tetrahedron of metal atoms must lie in either a right- or left-handed orientation.[5] When two octants share a face the two $M_4$ tetrahedra, one right- and one left-handed, will share a common edge across the diagonal of the contiguous octant faces. If for convenience we refer to the right- and left-handed orientation of the octants as δ and λ then each octant of δ phasing is circumscribed by six octants of

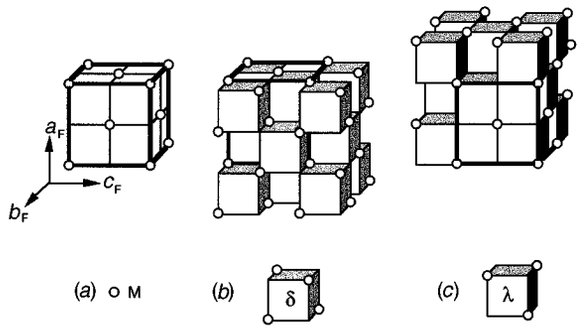


**Fig. 3** (*a*) Fluorite unit cube (bold outline). (*b*) Interpenetrating octant sub-lattice of the δ phase. (*c*) Interpenetrating sub-lattice of the λ phase

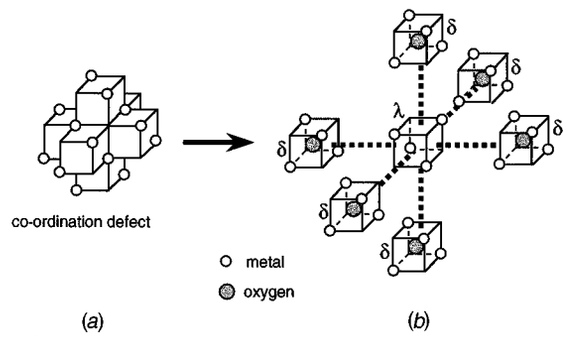


**Fig. 4** (*a*) Co-ordination defect showing characteristic topology. (*b*) Exploded view of c.d. showing the untenanted central octant of the λ phase co-ordinated by six $M_2O$ octants of the δ phase

the opposing λ phasing and *vice versa*; *i.e.* the metal phasing of the octants alternates along the $\langle 100\rangle_F$ directions. It follows that the fluorite structure [see Fig. 3(*a*)] can be viewed with greater prescience in terms of two interpenetrating f.c.c. sub-lattices comprised of octants with opposed metal phasing, δ [Fig. 3(*b*)] and λ [Fig. 3(*c*)]. The two octant sub-lattices must be equal in charge and symmetry. In this 1974 oxygen-centred perspective of fluorite lies the origin of the 'new' treatment by Eyring and co-workers of fluorite in terms of three interpenetrating f.c.c. lattices, one of cations and two of anions [*cf.* Fig. 4(*b*), ref. 6; Fig. 1(*b*), ref. 7; and Fig. 7, ref. 14].

Since the oxygen origins of the two octant sub-lattices lie at $x = \frac{1}{4}, \frac{1}{4}, \frac{1}{4}$ and $-\frac{1}{4}, -\frac{1}{4}, -\frac{1}{4}$ (see Fig. 3), a metal-centred (δ, λ) octant pair such as that along $\frac{1}{2}[1\bar{1}\bar{1}]_F$ can be regarded as the fundamental motif of the fluorite structure [see Fig. 2(*d*)]. This is again the octant origin of Eyring and co-workers 'mosaic group', O′–R–O (*cf.* Fig. 7, ref. 14). Clearly, the unit cell of fluorite can be assembled from the four such octant (δ, λ) pairs, each of composition $MO_2$, and oriented along one of the four $\langle 111\rangle$ axes of the unit cube [see Fig. 2(*b*)].

## Fluorite with one or two Vacancies

Removal of $O^{2-}$ from an octant centre generates a vacant site in the oxygen sub-lattice according to equation (1) where the

$$4M^{4+} + O^{2-}/\square_{an} \longrightarrow 4M^{4+} + 2e^-/\square_{an} + \tfrac{1}{2}O_2 \longrightarrow 2M^{4+} + 2M^{3+} + \square_{an} + \tfrac{1}{2}O_2 \quad (1)$$

symbol $\square_{an}$ designates an anion site denuded of oxygen. It is now well established that the true defect $\square_{an}$ does not exist in isolation in the fluorite lattice but is constituted of seven octants, a central octant $M_4\square$ which contains the vacancy and the six $M_4O$ octants which circumscribe it along the $\langle 100\rangle_F$ directions (see Fig. 4). It will be evident from Fig. 4 that the co-ordinated defect can be either right- or left-handed depending on the metal phasing of the central octant, and will possess the composition $M_{28/8}\square O_6$, *i.e.* $M_{3.5}\square O_6$ or $MO_{1.714}$. It is significant that the composition of this entity corresponds exactly to

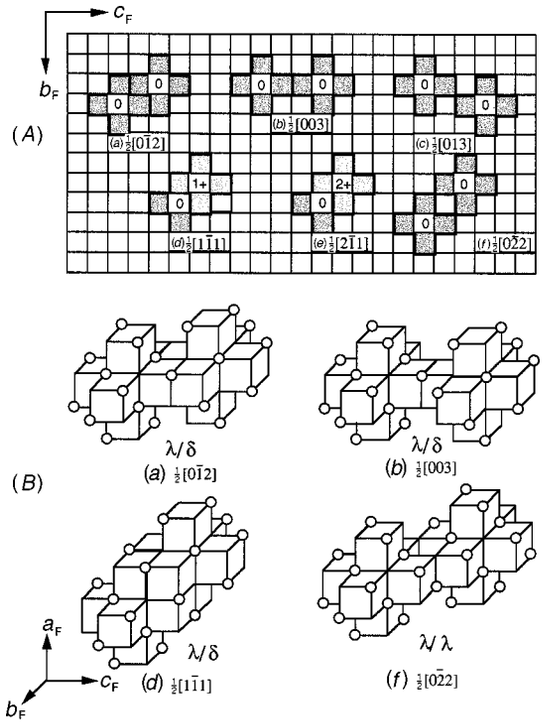


**Fig. 5** (*A*) Some anion vacancy–vacancy distances determined by permitted c.d.–c.d. contacts projected on the $(100)_F$ matrix. (*B*) Some allowed c.d.–c.d. contacts illustrated in three dimensions

that of the ordered intermediate lanthanoid oxide of greatest thermal stability, namely the ι phase, $M_7O_{12}$ with $n = 7$.

The presence of a co-ordinated vacant anion site in fluorite can be conveniently represented in a $(100)_F$ layer by shading its four nearest neighbouring octants as illustrated in Fig. 5(*A*). The two axial octants which complete a c.d. located in the $X = 0$ layer of necessity project into the adjoining octant layers situated above ($X = 1$) and below ($X = -1$) the vacant anion site. Conversely mating holes, H, are required in the $X = 0$ layer to accommodate the axially oriented octants of each c.d. located in the layers above ($X = 1$) and below ($X = -1$) the reference $X = 0$ layer. These mating holes in the $X = 0$ layer have been designated previously[1] as $H^+$ (*i.e.* a c.d. in the $X = 1$ layer) and $H^{-1}$ (*i.e.* a c.d. in the $X = -1$ layer). This terminology will be simplified here by deleting the symbol H and designating the location of any c.d. by its value of $X$ [*e.g.* see Fig. 5(*A*)(*d*) and 5(*A*)(*e*)]. This refinement of the original 1974 symbolism has the advantage that the location of a c.d. in any octant layer can be identified by employing the symbol $X+$ or $X-$, *i.e.* the relative height of an octant layer on the $a_F$ axis. The reference level is normally chosen at $X = 0$ and is designated simply either by zero or by a small circle.

For lanthanoid oxides with $n > 6$ the closest distance of approach for two c.d.s is determined by their topology within any single octant layer. This prevents any two anion vacancies being situated at $\frac{1}{2}\langle 011\rangle_F$ or $\frac{1}{2}\langle 001\rangle_F$. The closest distance of approach for such a pair is $\frac{1}{2}\langle 012\rangle_F$ in which two c.d.s share three common faces [see Fig. 5(*A*)(*a*) and 5(*B*)(*a*)]. The next-nearest distance is $\frac{1}{2}\langle 003\rangle_F$ achieved by sharing one common face [see Fig. 5(*A*)(*b*) and 5(*B*)(*b*)]. If two c.d.s share a common edge the resulting distance is $\frac{1}{2}\langle 013\rangle_F$ [see Fig. 5(*A*)(*c*)], whereas if two edges are shared the vacancies are separated by $\frac{1}{2}\langle 022\rangle_F$ [see Fig. 5(*A*)(*f*) and 5(*B*)(*f*)].

Thus the distinctive octahedral topology of the c.d. plays a dominant role in determining the number of ways in which successive octant layers of composition $MO_x$ can be arranged in a close-packed assembly and yet preserve the f.c.c. metal lattice. For example, if two contiguous octant layers were considered, say at $X = 0$ and 1, the closest distance of approach between vacant sites would be $\frac{1}{2}\langle 111\rangle_F$ which corresponds to

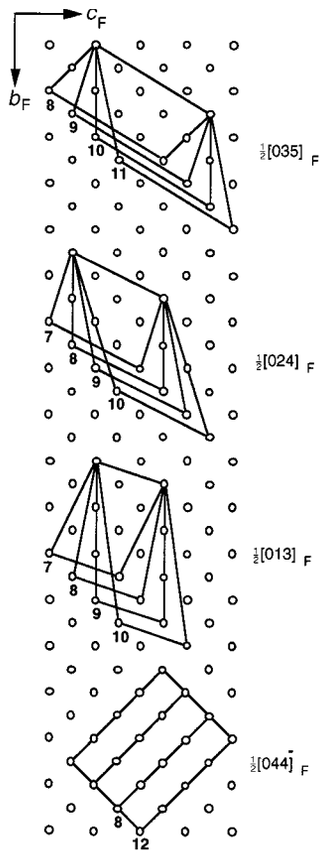


| $n$ | $\frac{1}{2}[035]_F$ |
|---|---|
| 7 | $\frac{1}{2}[042]$ or $\frac{1}{2}[0\bar{1}3]$ or $\frac{1}{2}[0\bar{2}8]$ |
| 8 | $\frac{1}{2}[053]$ or $\frac{1}{2}[022]$ or $\frac{1}{2}[0\bar{1}7]$ |
| 9 | $\frac{1}{2}[064]$ or $\frac{1}{2}[031]$ or $\frac{1}{2}[006]$ |
| 10 | $\frac{1}{2}[075]$ or $\frac{1}{2}[040]$ or $\frac{1}{2}[0\bar{1}5]$ |
| 11 | $\frac{1}{2}[086]$ or $\frac{1}{2}[051]$ or $\frac{1}{2}[024]$ |

| $n$ | $\frac{1}{2}[024]_F$ |
|---|---|
| 7 | $\frac{1}{2}[053]$ or $\frac{1}{2}[03\bar{1}]$ or $\frac{1}{2}[0\bar{1}5]$ |
| 8 | $\frac{1}{2}[064]$ or $\frac{1}{2}[040]$ or $\frac{1}{2}[024]$ |
| 9 | $\frac{1}{2}[075]$ or $\frac{1}{2}[051]$ or $\frac{1}{2}[033]$ |
| 10 | $\frac{1}{2}[086]$ or $\frac{1}{2}[062]$ or $\frac{1}{2}[042]$ |

| $n$ | $\frac{1}{2}[013]_F$ |
|---|---|
| 7 | $\frac{1}{2}[051]$ or $\frac{1}{2}[04\bar{2}]$ or $\frac{1}{2}[03\bar{5}]$ |
| 8 | $\frac{1}{2}[062]$ or $\frac{1}{2}[05\bar{1}]$ or $\frac{1}{2}[04\bar{4}]$ |
| 9 | $\frac{1}{2}[073]$ or $\frac{1}{2}[060]$ or $\frac{1}{2}[05\bar{3}]$ |
| 10 | $\frac{1}{2}[084]$ or $\frac{1}{2}[071]$ or $\frac{1}{2}[06\bar{2}]$ |

| $n$ | $\frac{1}{2}[044]_F$ |
|---|---|
| 8 | $\frac{1}{2}[06\bar{2}]$ or $\frac{1}{2}[022]$ or $\frac{1}{2}[02\bar{6}]$ |
| 12 | $\frac{1}{2}[07\bar{1}]$ or $\frac{1}{2}[033]$ or $\frac{1}{2}[0\bar{1}7]$ |
| 16 | $\frac{1}{2}[080]$ or $\frac{1}{2}[044]$ or $\frac{1}{2}[008]$ |
| 20 | $\frac{1}{2}[091]$ or $\frac{1}{2}[055]$ or $\frac{1}{2}[019]$ |

**Fig. 6** Some vectors characteristic of the $(100)_F$ structural repeat units for $M_nO_{2n-2}$ phases with different values of $n$.

the sharing of six common faces by two c.d.s [see Fig. 5(*A*)(*d*) and 5(*B*)(*d*)]. It is of considerable interest that only one unit-cell axis is common to the rhombohedral ($n = 7$), the triclinic ($n = 9$ and 11) and monoclinic ($n = 10$ and 12) binary oxides, namely $\frac{1}{2}\langle 211\rangle_F$. Three octant layers are necessarily involved, *i.e.*, $X = 0$, 1 and 2, and the common $\frac{1}{2}\langle 211\rangle_F$ vector corresponds to the closest possible distance that can be achieved between any two c.d.s (sharing five common edges) with the same metal phasing [see Fig. 5(*A*)(*e*)]. Within a single octant layer, the shortest vector with the same metal phasing is $\frac{1}{2}\langle 022\rangle_F$ [see Fig. 5(*A*)(*f*) and 5(*B*)(*f*)]. Some vectors often found in the $\{100\}_F$ structural repeat units for the homologous $M_nO_{2n-2}$ series are listed in Fig. 6.

When the unit cell of a defect fluorite phase ($n > 6$) contains two vacant sites, their closest distance of approach is $\frac{1}{2}\langle 111\rangle_F$ since the closer alternatives $\frac{1}{2}\langle 001\rangle_F$ and $\frac{1}{2}\langle 011\rangle_F$ are topologically excluded. The c.d. pair illustrated in Fig. 5(*B*)(*d*) is metal-centred along $\frac{1}{2}\langle 1\bar{1}1\rangle_F$ and possesses $D_{3d}$ point-group symmetry. Alternatively, if the two c.d.s forming the pair lie along the $\frac{1}{2}\langle 1\bar{1}\bar{1}\rangle_F$ direction, the two vacant octants no longer share a metal atom although the point-group symmetry is maintained. Eyring and co-workers[6,14] have employed operose electrostatic screening and charge-separation arguments to argue that the latter is the more stable configuration for a pair of anion vacancies along $\frac{1}{2}\langle 111\rangle_F$.

## Prediction of Defect Fluorite-related Structures

### (*a*) In the absence of unit-cell data

It was shown[5] that the existence of a homologous series of discrete ordered lanthanoid oxides of composition $M_nO_{2n-2}$ could be understood if $y$ octants of $M_2O$ were added successively to a c.d. of composition $M_{3.5}\square O_6$, the resulting composition of each phase then becoming $M_{3.5+0.5y}\square O_{6+y}$; *i.e.* $M_nO_{2n-2}\square_2$ with $n = y + 7$. In the absence of crystallographic information on the symmetry and dimensions of the various unit cells, it was proposed[5] that plausible superstructures for this extended series of phases could be predicted from a consideration of (a) the number of metal atoms $n$, (b) the value of $y$ (*i.e.* the composition $MO_x$), (c) recognition of the correct phasing of the metal lattice and (d) the geometrical restrictions demanded by the topology of the c.d. Of the five phases studied recently by neutron diffraction,[10–13] the ordering of anion vacancies in the $\{001\}_F$-type layers predicted for the homologues $n = 7$ and 11 predicted[5] were confirmed; those for $n = 9$, 10 and 12 proved to be incorrect. In retrospect this arose because at that time the number of alternative ways in which $n$ metal atoms can be enclosed by a regular repeat unit in a $\{100\}_F$ layer was not fully explored. Some examples of the wide range of possible repeat units for different values of $n$ which can arise from commonly observed vectors in fluorite-related structures are illustrated in Fig. 6. It is noteworthy that all the vectors which were chosen to define both the sides and diagonals of the $\{001\}_F$-type repeat units predicted *ab initio* in 1974 (see Figs. 5 and 8 of ref. 5) are represented in the tables of Fig. 6. At that time it was postulated that for all the homologues the c.d.s would be close-packed with the $\frac{1}{2}\langle 012\rangle_F$ spacing to generate rows incorporating a common cell edge of $\frac{1}{2}\langle 024\rangle_F$ (*cf.* Figs. 4 and 8, ref. 5). Whereas the recently published neutron diffraction data[10–13] indicate this to be true for only two of the five homologues, namely $n = 7$ and 11, nevertheless $\frac{1}{2}\langle 012\rangle_F$ stands out as the dominant vector between c.d.s in all the known oxide structures (*cf.* Figs. 5, 13, 17, 21 and 27, ref. 1).

### (*b*) In the presence of unit-cell data

Eyring and Kang[6,7] have acknowledged the correctness of the co-ordination defect but claim[6] 'what is missing in their (*i.e.* Hoskins and Martin) discussion is the underlying structural principle and the ability to predict unknown structures of the homologues series members, their polymorphs, and an integration of all known intermediate phases into a single series'. In order to demonstrate that this criticism is undeserved it is necessary to elaborate here the methodology used by Hoskins and Martin[9] in 1976 to predict the possible structures for the rhombohedral and triclinic homologues ι-$M_7O_{12}$, ζ-$M_9O_{16}$ and δ-$M_{11}O_{20}$ using the published[8] symmetry and unit-cell parameters determined from electron diffraction of very small crystals. To achieve this it is convenient to follow Eyring and co-workers[6,14] presentation and formalize our topological analysis methodology in terms of a series of rules. It should be noted that diffraction experiments on some fluorite-related oxides have revealed unit cells which correspond to large superstructures containing multiples of the two vacant anion sites in the homologous formula $MnO_{2n-2}$. This multiplicity is readily accommodated in the generic formula developed above by simply combining $m$ c.d.s (rather than one) with $y$ octants of composition $M_2O$ to obtain the composition $M_{(3\frac{1}{2}m+\frac{1}{2}y)}O_{(6m+y)}\square_m$; *i.e.* $M_nO_{2n-2m}\square_{2m}$ where $n = 7m + y$ and $m$ takes integral values greater or equal to one. For a phase of general composition $MO_x$ it follows that $nx = 2n - 2m$ or $m = n - \frac{1}{2}nx$ as reported by Kang and Eyring.[6] If $n$ is known from diffraction experiments, then the vacant site multiplicity $m$ can be calculated from a knowledge of the chemically determined composition of the phase, $MO_x$.

**The c.d. rules.** (1) The octant of the fluoride unit cell of composition $M_2O$, is chosen as the fundamental module with which to model the structures. It may possess either right-(δ) or left-(λ) handedness [*cf.* Fig. 2(*b*)]. (2) Each vacant oxygen site possesses a local environment of six octahedrally disposed oxygen anions and four tetrahedrally disposed metal cations to form a co-ordination defect of composition $M_{3.5}\square O_6$. The topology of this c.d. is structure determining (*cf.* Fig. 4). (3) Two c.d.s in any member structure cannot be closer than the body diagonal of

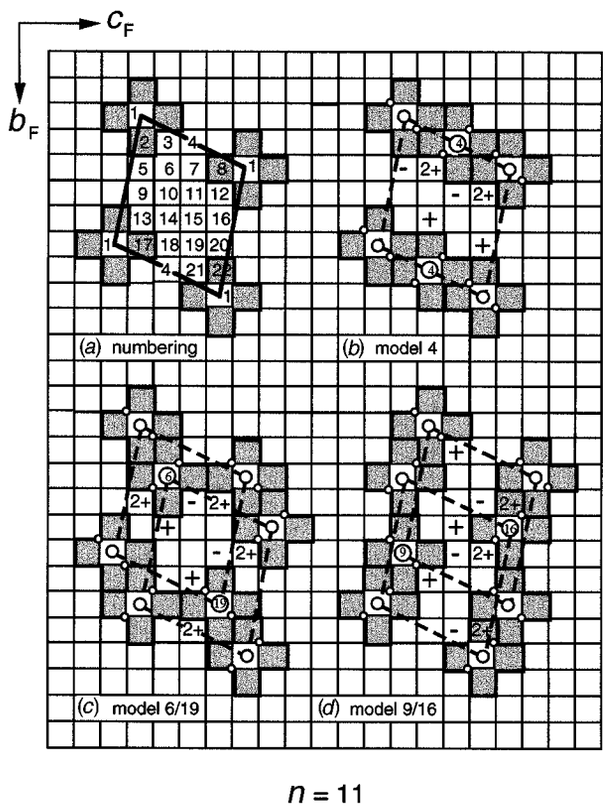


**Fig. 7** Predicted models for δ-$M_{11}O_{20}$. Octant numbering system (*a*) and structural repeat units in the $(100)_F$ layer for models 4 (*b*), 6/19 (*c*) and 9/16 (*d*)

the simple cubic oxygen array, *i.e.* $\frac{1}{2}\langle 111\rangle_F$ [*cf.* Fig. 5(*A*)(*d*) and 5(*B*)(*d*)]. (4) Define a repeat unit in a $\{100\}_F$ layer of octants containing *n* metal atoms which is consistent with the crystallographic unit-cell data [*e.g.* see Figs. 6 and 7(*a*)]. This is achieved from a knowledge of the relationship between the true unit cell and the fluorite cell and subsequent vector addition or subtraction to determine appropriate vectors in the {100} fluorite plane. (5) Assign c.d. 1 to the corners of the repeat unit in the octant layer at $X = 0$ and reject all octant sites which are closer to vacancy 1 than $\frac{1}{2}\langle 012\rangle_F$ as potential sites for the deployment of c.d. 2. (6) Eliminate all remaining octant sites which possess the same metal phasing as that of c.d. 1; *i.e.* the second c.d. must occupy a site of the opposite metal phasing. (7) Locate c.d.s in the adjoining octant layers at $X = +1/-1$, $+2/-2$, *etc.* by using the appropriate unit-cell transformation matrices. Reject any site in the octant layer at $X = 0$ which is closer than $\frac{1}{2}\langle 102\rangle_F$ to a c.d. located in the adjoining octant layer at $X = +1$ or $-1$, *etc.*

The methodology for applying these rules is illustrated below for the largest triclinic homologue, δ-$M_{11}O_{20}$, for which the structure is known.[11] The systematic topological analysis reveals that there are only three predicted structures compatible with the unit-cell characteristics. For example, the repeat unit in the $(100)_F$ octant layer at height $X = 0$ is first derived from the crystallographically determined[11] transformation matrix $a = a_F + \frac{1}{2}b_F - \frac{1}{2}c_F$, $b = -\frac{1}{2}a_F + \frac{3}{2}b_F + c_F$ and $c = \frac{1}{2}a_F - \frac{1}{2}b_F + c_F$ which enables the supercell for the triclinic $n = 11$ phase to be related to the fluorite sub-cell [Fig. 7(*a*) and rule 4]. In Fig. 7(*a*) the first vacancy (or c.d.) is assigned to the four corners (*i.e.* octant 1) of the repeat unit and arbitrarily given δ phasing. The topology of c.d. 1 excludes as potential sites for the second vacancy the octants numbered 1–3, 5, 7, 8, 12, 13, 17, 18, 20–22 (rule 5). Of the remaining octants 4, 6, 9–11, 14–16, 19, those situated at positions 10 and 15 can be eliminated because they have the same phase, δ, as octant 1 (rule 6). The c.d.s in the adjoining octant layers at $X = 1$ and $-1$ can be located at sites 14 (designated +) and 11 (designated −) by applying either the *b* or *c* displacement vector to c.d. 1 in the layer at $X = 0$. Occupancy of site 14 by a c.d. situated in the octant layer at $X = 1$ eliminates the octants 10, 13–15 and 18, and occupancy of site 11 at $X = -1$ eliminates octants 7, 10–12 and 15 due to respective topological requirements of the five c.d.s involved in each case (rule 7). The sites with λ phasing which remain for accommodating the second c.d. are then 4, 6, 9, 16 and 19.

If the second c.d. occupies position 4, the resulting structure [Fig. 7(*b*)] is one of the three predicted in 1976 and recently confirmed[11] by high-resolution neutron diffraction of powdered samples. The structure involves isolated anion vacancies and it is noteworthy that the $(100)_F$ repeat unit for model 4 is identical to that predicted in 1974 for the $n = 11$ phase [Fig. 8(*d*), ref. 5] based on c.d. topology alone, there being no crystallographic data for this phase available at that time to guide the way in which the successive $(100)_F$ layers might be stacked.

When the second c.d. is located at either positions 6 or 19 it will be evident from Fig. 7(*c*) that two equivalent repeat units can be drawn for the c.d. pair 6/19 with both representing the predicted structure. For example in model 6 the corners of one repeat unit are assumed to be occupied by c.d. 1 with δ phasing so that the second c.d. numbered 6 possesses λ phasing. In the alternative unit, model 19, the corners now occupied by c.d. 6 are necessarily of λ phasing so that c.d. 19 must possess δ phasing as required by rule 6. Similarly, the two equivalent repeat units delineated for model 9/16 represent the single model structure illustrated in Fig. 7(*d*). Thus, when taken together with model 4, the above topological analysis has reduced to three the number of trial defect structures possible for the $n = 11$ oxide phase; these are the same structural models predicted and discussed[9] previously. Model 9/16 has the same distribution of c.d.s as that illustrated in Fig. 6(*a*) of ref. 9 and involves metal-centred anion vacancy pairs oriented along the $[111]_F$ direction [Fig. 7(*d*)]. On the other hand model 6/19 involves metal-centred vacancy pairs in the alternative orientation, $[1\bar{1}\bar{1}]_F$, as shown in Fig. 7(*c*). The vector $\frac{1}{2}\langle 111\rangle_F$ occurring in these two models reflects the closest distance of approach possible for two c.d.s and is consistent with rule 3.

Application of the above rules to the other (*i.e.* $n = 7$ and 9) homologues yields a unique model for the rhombohedral ι-$M_7O_{12}$ phase which is the crystallographically determined[11,15] structure (see Fig. 5, ref. 5 and Fig. 5, ref. 1). In the case of the triclinic ζ-$M_9O_{16}$ phase the c.d. rules reduce to two the number of predicted models which are compatible with the topological requirements of the c.d. and the unit-cell data. The actual structure (model 8/17) is sketched in Fig. 8(*b*) and has pairs of discrete metal-centred c.d.s along the [111] direction. The alternative model [Fig. 8(*d*)] results in an arrangement of c.d.s such that the vacant octants form strings along $[1\bar{1}\bar{1}]_F$.

It is noteworthy that the $(100)_F$ repeat units of the rhombohedral $n = 7$ and triclinic $n = 11$ phases both involve parallel sides with either the vector $\frac{1}{2}[0\bar{2}1]_F$ or $\frac{1}{2}[012]_F$, respectively. It might therefore be unexpected that the intermediate homologue with $n = 9$ is bounded by the different vectors $\frac{1}{2}[006]_F$ and $\frac{1}{2}[031]_F$. The reason for this is that it is impossible to construct an ι-type repeat unit for the $n = 9$ phase based on parallel sides with the $\frac{1}{2}[012]_F$ vector. If this were attempted [see Fig. 8(*c*)] it would be found that the common $a = \frac{1}{2}[21\bar{1}]_F$ (which locates c.d.s at 2+) and $c = \frac{1}{2}[1\bar{1}2]_F$ (which locates c.d.s at 1+) vectors would not be commensurate (*cf.* rule 7). This problem is overcome in the real structure by restricting the run of c.d.s along the $\frac{1}{2}[012]_F$ direction to c.d. pairs separated from their nearest neighbours by either $\frac{1}{2}[006]_F$ or $\frac{1}{2}[031]_F$ in the actual repeat unit [see Fig. 8(*b*)].

Not surprisingly the task of modelling fluorite-related structures becomes more formidable as the value of *m* in the generic formula and the size of the unit cell increases. Even so, the above rules for predicting model structures can be applied[16]

with equal confidence to much larger phases such as the triclinic binary oxide, $Ce_{19}O_{34}$, with $n = 19$ and $m = 2$ (see below).

### (*c*) Modelling an unknown structure with $n = 8$

Eyring and co-workers[6,14] have claimed that a special strength of their phenomenological structural principles is the ability to predict structures not yet established. From this point of view one of the more intriguing features of the homologous $M_nO_{2n-2}$ series of oxides in the region $M_7O_{12}$ to $MO_2$ is the apparent absence of the second member $M_8O_{14}$. An ordered phase of this composition was not detected[17] in isobaric and tensimetric studies of the $PrO_x$–$O_2$ system even though $Pr_8O_{14}$ would not be expected to decompose peritectoidally until the relatively high temperature of *ca.* 950 K if it were to exist (see Fig. 10 of ref. 5). Nevertheless, it is relevant that many of the $(011)_F$ planes in monoclinic ε-$Pr_{10}O_{18}$ and β-$Pr_{12}O_{22}$ actually do have the composition $Pr_8O_{14}$. On this basis Hoskins and Martin[1] concluded that if such a phase were to exist it would probably also be monoclinic but with a smaller unit cell of relative volume equal to two. Such a conjectural phase would then become the first member of the even-*n* homologues with the same *a* and *c* axes and therefore should be related to the fluorite lattice of $PrO_2$ by the transformations $a = a_F + \frac{1}{2}b_F - \frac{1}{2}c_F$, $b = b_F + c_F$ and $c = a_F - \frac{3}{2}b_F + \frac{3}{2}c_F$.

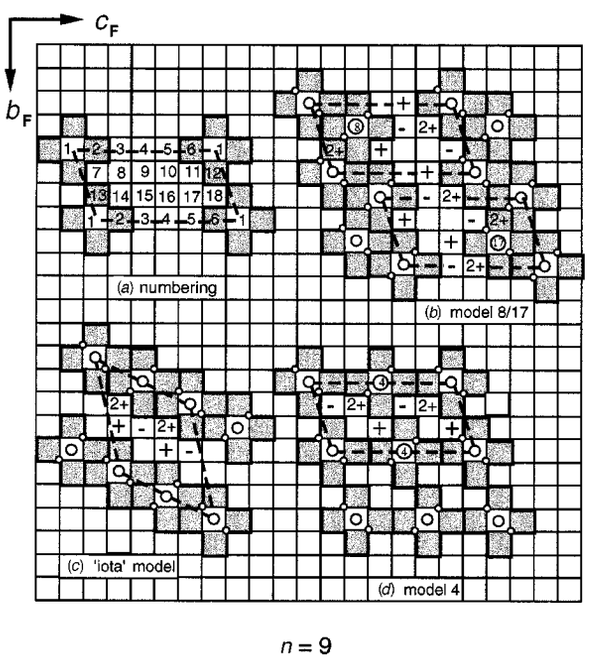


**Fig. 8** Predicted models for ζ-$M_9O_{16}$. Octant numbering system (*a*) and structural repeat units in the $(100)_F$ layer for models 8/17 (*b*) 'iota' (*c*) and 4 (*d*)

Kang and Eyring[6] using their phenomenological structural principles have concluded that, although a compound with the composition $M_8O_{14}$ can be modelled by utilizing the eight possible vacancy orientations of their $M_4O_7$ module, 'it is geometrically impossible to fill two-dimensional space with it'. Nevertheless it seems surprising that fluorite-related phases with $n = 7$ and 9 can be modelled successfully whereas the intermediate member with $n = 8$ cannot. Indeed the application of the c.d. rules to the unknown monoclinic $n = 8$ phase leads to the two alternative models illustrated in Fig. 9(*b*) and 9(*c*). Model 6/15 would involve the second c.d. at either position 6 or 15 whereas model 10/12 would place the second c.d. at either position 10 or 12. The two equivalent repeat units shown for each of the models 6 and 15 [Fig. 9(*b*)] describe the same $(100)_F$ trial structure. Likewise the repeat units for models 10 and 12 can be delineated on the alternative common $(100)_F$ structure [Fig. 9(*c*)].

The unit-cell transformations given above require both the models 6/15 and 10/12 to be characterized by the $[21\bar{1}]_F$ unit cell vector of the ι-phase and to possess a common $(011)_F$ plane which is defined by their identical *a* and *c* axes. Examination of Fig. 9(*b*) and 9(*c*) reveals that a structure in three dimensions for $M_8O_{14}$ can be constructed if two types of alternating $(100)_F$ layer, say A and B, each possessing a different arrangement of c.d.s, were stacked along the $a_F$ axis so that the next but one layers A–A (or B–B) would be displaced by the $\frac{1}{2}[21\bar{1}]_F$ vector. The required B layers are illustrated for $X = +1$ and $-1$ in Fig. 10(*b*) and 10(*c*) and are comprised of $\frac{1}{2}[0\bar{1}2]_F$ and $\frac{1}{2}[030]_F$ related c.d.s whereas the A layer at $X = 0$ (or $X = 2+$ or $2-$) in Fig. 10(*a*) involves $\frac{1}{2}[0\bar{2}1]_F$ and $\frac{1}{2}[003]_F$ c.d. nearest neighbours. Inspection of Fig. 9(*b*) and 9(*c*) reveals that the A and B $(100)_F$ octant layers are just those which characterize the predicted model structures 6/15 and 10/12; *i.e.* the B layers at $X = +1$ and $-1$ are those of model 10/12 whereas the A layer at $X = 0$ is that of model 6/15. The individual A or B octant layers are repeated up the $a_F$ axis for the values of $X = 0, 8, 16, \ldots$ *etc*. These same structural characteristics have been identified previously[1] for

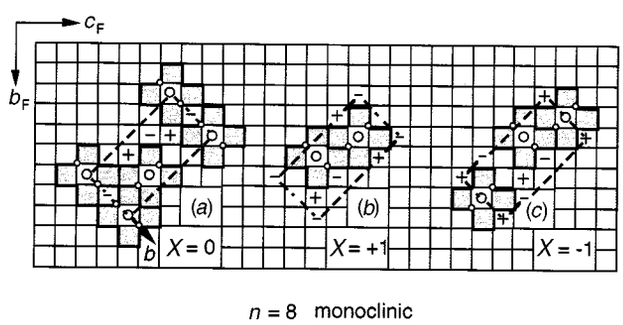


**Fig. 10** Three adjoining $(100)_F$ octant layers of $M_8O_{14}$ showing (*a*) the monoclinic *b* axis and a unit of composition $M_8O_{14}\square_2$ at $X = 0$, and two adjoining layers (*b*) and (*c*) at $X = +1$ and $-1$

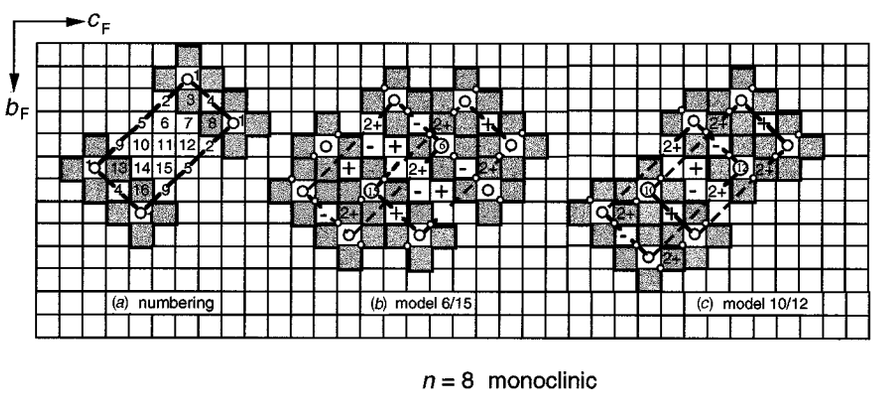


**Fig. 9** Predicted models for the unknown $M_8O_{14}$ monoclinic phase. Octant numbering system (*a*) and structural repeat units in the $(100)_F$ layer for models 6/15 (*b*) and 10/12 (*c*)

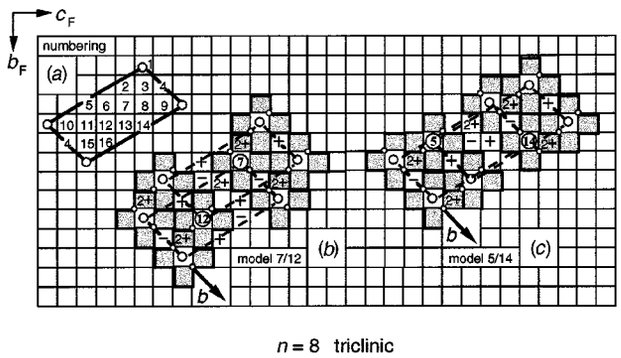


**Fig. 11** Predicted model for the unknown $M_8O_{14}$ triclinic phase. Octant numbering system (*a*) and structural repeat units in the $(100)_F$ layer for models 7/12 (*b*) and 5/14 (*c*)

the monoclinic ε-$Pr_{10}O_{18}$ and β-$Pr_{12}O_{22}$ phases. Thus the application of the c.d. rules leads to a unique monoclinic structure predicted for $M_8O_{14}$ which can be packed without any problems, not only in two but in all three directions (see below). This successful prediction highlights the shortcomings of the Eyring phenomenological structural principles for predicting trial structures for unknown phases.

In view of Eyring's conviction that a compound with the composition $M_8O_{14}$ within the region of stable fluorite-related phases is impossible to model under their rules, it is important to demonstrate that two conjectural triclinic polymorphs can also be predicted using the c.d. theory. Thus if the diagonal of the above monoclinic repeat unit were moved from $\frac{1}{2}[0\bar{6}2]_F$ to $\frac{1}{2}[0\bar{5}3]_F$, the $(100)_F$ triclinic repeat unit illustrated in Fig. 11(*a*) would be generated for $M_8O_{14}$. Application of the c.d. rules to this unit (see above) reduces the number of predicted structures to two, one with the second c.d. located at positions 7 or 12 [see Fig. 11(*b*)] and the other at position 5 or 14 [see Fig. 11(*c*)]. The c.d. motif for model 7/12 is characterized by the vectors $\frac{1}{2}[0\bar{2}1]_F$ and $\frac{1}{2}[003]_F$, *i.e.* vectors identical to those of the motif of the A layer found for the monoclinic model 6/15. However, the repeat units for the monoclinic and triclinic models differ in that the motifs comprising each of the $(100)_F$ layers are displaced by the vector $\frac{1}{2}[011]_F$ due to the shift of the cell diagonal.Model 7/12 can be related to the fluorite lattice of $MO_2$ by the transformations, $a = a_F + \frac{1}{2}b_F - \frac{1}{2}c_F$, $b = b_F + c_F$ and $c = \frac{1}{2}a_F - \frac{1}{2}b_F + c_F$. In this modification the locations of c.d.s in the octant layer at $X = 1$ or $-1$ are defined by the *c* axis of the unit cell whereas those at $X = 2$ or $-2$ are determined by the *a* axis. The stacking of four adjoining layers at $X = -1$, 0, 1 and 2 shown in Fig. 11(*b*) produces a structure that geometrically fills all three dimensions and gives the correct composition for a triclinic $n = 8$ phase.

The c.d. motif for the triclinic model 5/14 involves the alternative vectors $\frac{1}{2}[0\bar{1}2]_F$ and $\frac{1}{2}[030]_F$, *i.e.* identical to those of the motif that characterizes the B layer for the monoclinic model 10/12 in Fig. 9(*c*). Model 5/14 can be related to the fluorite lattice of $MO_2$ by the same *a* and *b* but a different *c* transformation, namely, $c = \frac{1}{2}a_F - b_F + \frac{1}{2}c_F$. This alternative polymorph is depicted in Fig. 11(*c*). Again the stacking of these $(100)_F$ layers of octants along $a_F$ produces a structure that fills three-dimensional space and gives the correct composition $M_8O_{14}$ for a model triclinic $n = 8$ phase (see below).

The close relationship between the cubic pyrochlore structure (which is found in a number of ternary oxide systems with compounds such as $Gd_4Zr_4O_{14}$) and fluorite has been alluded to elsewhere.[5,18] If a $(100)_F$ layer of pyrochlore [see Figs. 13 and 16(*a*), ref. 18] were compared to those of either the monoclinic or triclinic models for $M_8O_{14}$, it would be seen that strings of metal-centred c.d.s along the $[011]_F$ direction were common to all three structures. A series of co-operative shear displacements of $(0\bar{1}1)_F$ planes would suffice to transform either of the fluorite-related polymorphs into the pyrochlore structure. Since none of the predicted model structures nor the pyrochlore structure has been observed for binary lanthanoid oxides of this composition the reason for their absence remains obscure.

## Fluorite-type Modules

The 'new' phenomenological structural principles, and rules for their application, advanced by Eyring and co-workers[6,14] for predicting the ideal structures of the intermediate lanthanoid oxides are predicated on using the fluorite unit cell as the primary building block or module. Subsiduary modules are then derived from the primary module by introducing one or two vacant oxygen sites. Providing that the way in which an adjoining pair of fluorite modules can be placed in juxtaposition can be uniquely determined, the constitution of members of the homologous series $M_nO_{2n-2m}\square_{2m}$ can then be expressed in terms of the specific packing sequences for the *n* modules required to characterize each homologue.

In order to evaluate their proposal that the fluorite unit cell should be the primary module on which to base the prediction of fluorite-related structures, it will be necessary first to compare the relative merits of several alternative and more primitive modules based on fluorite. It will emerge that fluorite module sequencing cannot be determined uniquely unless the topological constraints imposed by the co-ordination defect are properly taken into account. It will also be demonstrated that the operose electrostatic screening and electric dipole orientation arguments invoked by Eyring and co-workers[6,14] to define the directions of maximum ion–ion (or vacancy–vacancy) interaction, and to account for the eight possible and equally likely fluorite modules containing one anion vacancy, each with a different dipole orientation, are questionable and indeed, unnecessary.

### (*a*) The fluorite octant

In the c.d. theory[5] an octant of the unit cell of fluorite-related $M_4O_8$ is employed as the basic building block or primary module. The superstructures of the intermediate oxides can then be depicted in terms of c.d. diagrams from which the exact sequence of octant modules can be derived. For example, if the basic $M_2O$ module were designated by the symbol o, and a vacant octant by the symbol $o^0$, it would follow from Fig. 8(*b*) that the $n = 9$ phase could be reproduced along the $[011]_F$ direction for any octant layer by a pair of module sequences (one δ and one λ) of the type [ooooo$^0$oooo], each having the composition $M_{9/2}O_8\square$. An assembly of face-sharing octants based on the analogous $n = 7$ sequences was originally employed in Fig. 6(*a*) to illustrate[5] the three-dimensional structure of the ι-$M_7O_{12}$ phase.

### (*b*) The fluorite quadrant

The (δ, λ) pair of octants illustrated in Fig. 2(*e*) forms a quadrant of the fluorite cube of composition $MO_2$. Since each quadrant spans two adjoining octant layers say, $X = 0$ and 1, it can be represented by the icon $f_j^i$ with the four orientational variants being $(i, j) = (1, 3)$, $(2, 4)$, $(3, 1)$ and $(4, 2)$ where the octant numbering given in Fig. 2(*b*) is followed. If one octant of the quadrant were untenanted, a quadrant of composition $MO\square$ would be formed that could be designated by the icon $q^i$ if the vacant anion site were in the upper ($X = 1$) octant layer or $q_j$ if it were to lie in the lower ($X = 0$) layer. If both octants of the quadrant were vacant, the resulting module of composition $M\square_2$ would possess four $\frac{1}{2}\langle 111\rangle_F$ orientational variants as above and could be represented by $w_j^i$. Fluorite-related structures can be reproduced by intersecting strings comprising $f_j^i$, $q^i$, $q_j$ and $w_j^i$ corner-sharing modules along the four $\langle 111\rangle_F$ directions. For example, a typical sequence of nine quadrant modules along the $[111]_F$ direction for ζ-$M_9O_{16}$ can be derived from the c.d. diagram in Fig. 14(*a*) as $[q^4q_2f_2^4f_2^4f_2^4f_2^4f_2^4f_2^4]$ with the composition $M_9O_{16}\square_2$.

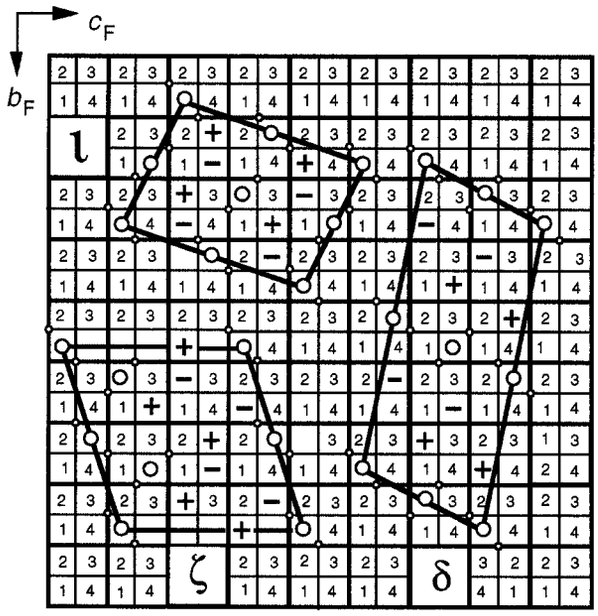


**Fig. 12** Matrix representation of a $(100)_F$ layer of fluorite octants grouped into quartets (bold outline) numbered 1–4 and of composition $M_2O_4$. Modular repeat units are delineated for ι-$M_7O_{12}$, ζ-$M_9O_{16}$ and δ-$M_{11}O_{20}$

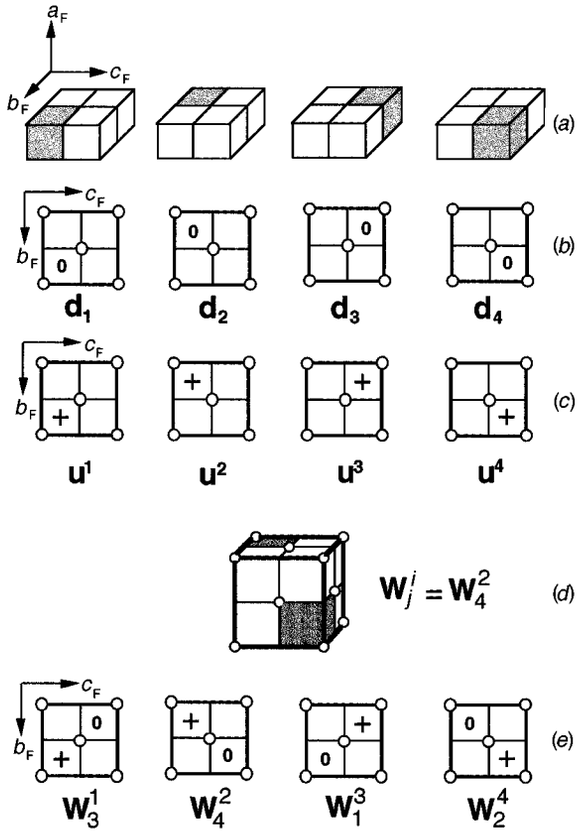


**Fig. 13** Representations of twelve of the thirteen fluorite hemicube modules from which all the binary lanthanoid oxides can be modelled. (*a*) Fluorite hemicubes containing one vacant oxygen site (shaded) with composition $M_2O_3\square$, (*b*) matrix representation of $d_j$ hemicube modules in $X = 0$ layer, (*c*) $u^i$ hemicube modules in $X = 1$ layer, (*d*) fluorite module $W_j^i$ of composition $M_4O_6\square_2$ and (*e*) four possible orientational variants of the $W_j^i$ module in matrix representation

It can be noted that there are several alternative quadrants that could have been chosen as the basic building module for the fluorite cube. One such example is the quadrant depicted in Fig. 2(*d*) comprising two octants (δ, λ) corner linked along $\frac{1}{2}\langle 111\rangle_F$ through a common metal atom. Alternatively, if a single fluorite $\{100\}_F$ octant layer were considered, the structure could be reproduced by one or more of several $MO_2$ quadrants comprising octant pairs sharing either an edge along $\frac{1}{2}\langle 011\rangle_F$ (*i.e.* δ, δ or λ, λ) or a face along $\frac{1}{2}\langle 100\rangle_F$ with (δ, λ) phasing.

### (*c*) The fluorite hemicube

The fluorite cube illustrated in Fig. 2(*a*) and 2(*b*) can also be considered as being comprised of a lower quartet of octants at $X = 0$ [numbered 1–4 in Fig. 2(*b*)] together with an equivalent upper set lying at $X = 1$. Effectively, each quartet of composition $M_2O_4$ is one half of the unit cell of fluorite and is termed here the fluorite hemicube and designated by the symbol f. Thus the matrix representation of a $(100)_F$ layer of octants shown in Fig. 2(*c*) can be elaborated further by depicting the fluorite lattice simultaneously as an assembly of octant quartets (numbered 1–4), *i.e.* f hemicubes (*cf.* bold squares in Fig. 12).

The hemicube can be regarded, as can the octant or quadrant, as a basic building block or module from which members of the homologous series of lanthanoid oxides may be constructed. If one member (shaded) of the quartet of octants contains an anion vacancy there will be four alternative modules formed of composition, $M_2O_3\square$ [see Fig. 13(*a*)]. These are designated $d_j$ ($j = 1$–4) for the $(100)_F$ layer at $X = 0$ and can be represented schematically by the matrix illustrated in Fig. 13(*b*). The adjoining octant layer at $X = 1$ will be comprised of either $M_2O_4$ or $M_2O_3\square$ modules which can likewise be designated as either f or $u^i$ ($i = 1$–4) [Fig. 13(*c*)]. For each homologue the repeat unit within any octant layer can be represented by sequences of these hemicubes sharing faces and packed into two-dimensional compositional slabs that can be aggregated to make up the three-dimensional structure.

The repeat units for the phases ι-$M_7O_{12}$, ζ-$M_9O_{16}$ and δ-$M_{11}O_{22}$ are delineated in Fig. 12 in such a way that the four corners of each unit are labelled octant 1 and arbitrarily given δ phasing of the metal atoms [as in Figs. 2(*b*) and 12]. Inspection of the repeat units for the octant layer at $X = 0$ reveals that the number of hemicube modules which defines each phase is 7, 9 and 11 respectively, *i.e.* the number of metal atoms $n$ as expected. The modular sequences and compositions for each phase can be read from Fig. 12 and at $X = 0$ are $[d_1fd_2d_4fd_3f] = M_{14}O_{24}\square_4$ and $[d_1fffd_3d_4ffffd_2] = M_{22}O_{40}\square_4$ along the $[001]_F$ and $[d_1d_2fffd_4ffd_3] = M_{18}O_{32}\square_4$ along the $[011]_F$, directions.

It is evident from Fig. 2(*b*) that each hemicube module comprises two octants of δ phase and two octants of λ phase which can be designated at $\delta_1$, $\delta_3$, $\lambda_2$ and $\lambda_4$. Since the two types of octant are present in equal numbers it follows that there must always be an even number of c.d.s present in the unit cell of any homologue as required by the formula $M_nO_{2n-2m}\square_{2m}$. An important consequence of the symmetry of the fluorite octant matrix as illustrated in Fig. 12 is that any regular quadrilateral repeat unit which encloses $n$ metal atoms must always contain the $d_1$, $d_2$, $d_3$ and $d_4$ (or $u^1$, $u^2$, $u^3$ and $u^4$) modules in equal numbers. This result follows from the geometry of the matrix and is unrelated to either the presumed orientation and dipole moment of each module or to the perceived requirement that the total structure should be dipole neutral.[6,14]

### (*d*) The fluorite module

The locations of c.d.s in the layer of hemimodules at $X = 1$ are designated by the symbol + in Fig. 12. For the triclinic ζ-$M_9O_{16}$ and δ-$M_{11}O_{20}$ phases every $d_j$ module at $X = 0$ is capped by an f module at $X = 1$. This combination of $d_j$ and f hemicubes yields a fluorite cube of composition $M_4O_7\square$ containing one vacant oxygen site, and this is the origin of the $D_j$ modules proposed by Kang and Eyring.[6] Similarly it is evident from Fig. 12 that each $u^i$ module at $X = 1$ of the ζ- and δ-oxide phases caps only f modules in the lower octant layer at $X = 0$ thereby generating

the corresponding $U^i$ modules of composition $M_4O_7\square$. The f modules at $X = 0$ which are capped by f modules at $X = 1$ become the F modules of composition $M_4O_8$ in the Eyring treatment. Inspection of the repeat unit for rhombohedral ι-$M_7O_{12}$ in Fig. 12 reveals the presence of a new type of fluorite module in which the vacancy in the lower $d_j$ hemicube bears a $\frac{1}{2}\langle 111\rangle_F$ relationship to the vacancy contained in the upper capping $u^i$ hemicube. There are four orientational variants of this circumstance which arise from the pairings $d_1$–$u^3$, $d_2$–$u^4$, $d_3$–$u^1$ and $d^4$–$u^2$. These four combinations are the fluorite modules containing two vacant anion sites designated by Eyring as $w_1^3$, $w_2^4$, $w_3^1$ and $w_4^2$ of composition $M_4O_6\square_2$, *i.e.* the composition of the lanthanoid sesquioxides, $M_2O_3$ [see Fig. 13(*d*) and 13(*e*)].

### (*e*) Modular sequencing and structures

The co-ordination defect theory not only provides a powerful method for predicting the number of possible models for any ordered phase but also enables the exact sequence of modules along all three axial directions for any defect fluorite phase of known or unknown structure to be determined. Not surprisingly, the efficacy of the c.d. method is not dependent on whether the parent module is an octant or quadrant of the fluorite cube, a fluorite hemicube, or a fluorite cube; all are congruent and commensurate both with the fluorite substructure and the superstructures of the intermediate lanthanoid oxides.

Application of the c.d. method is illustrated diagrammatically in Fig. 14 for the triclinic homologue, ζ-$M_9O_{16}$. The distribution of c.d.s over seven adjoining $(100)_F$ octant layers determined from the rules given above is provided in Fig. 14(*a*) for values of $X$ ranging from 3− to 3+. The number of octant layers represented by this type of c.d. diagram can readily be extended to include even higher and lower values of $X$. The sequence of hemimodules along an $[011]_F$ direction in Fig. 14(*a*) for the layer at $X = 0$ is seen to be $[fd_2fffd_4d_3d_1f]$ and for the layer at $X = 1+$ is $[ffu^3u^1u^2fffu^4]$ [see Fig. 14(*b*)]. Since each quartet of octants at $X = 1+$ caps the quartet immediately below at $X = 0$, the sequence of fluorite modules is identified as $[FD_2U^3U^1U^2D_4D_3D_1U^4]$ with the required composition $M_{36}O_{64}\square_8$ of the ζ phase. Furthermore, the manner in which fluorite modules can be stacked along the $a_F$ axis can also be unambiguously determined by identifying the hemimodule pairs of sequences at $X = +2/+3$ and $-1/-2$ as shown in Fig. 14(*b*) and 14(*c*). It will be noticed that while the fluorite module sequence remains unchanged along $[011]_F$, it becomes displaced for different heights along the $a_F$-axis [see Fig. 14(*c*)]. These vertical sequences also enable the fluorite modular sequence along the $[100]_F$ direction to be determined simultaneously and for the ζ phase is seen to be $[FD_2U^3U^1U^2D_4D_3D_1U^4]$, *i.e.* identical with the sequence along $[011]_F$.

If the c.d. diagram given in Fig. 14(*a*) were rotated by π/2 so that the $b_F$ axis becomes the abscissa, then the modular sequences along the $[010]_F$ direction become $[D_4U^2D_2D_1D_3FU^1U^3U^4]$. This sequence agrees with that listed in Table 5 of Kang and Eyring[6] providing the difference in choice of axes is taken into account (*i.e.* $[00\bar{1}]_F$ replaces $[100]_F$ of ref. 6). Further examination of the c.d. diagram [Fig. 14(*a*)] reveals that the three adjoining modular sequences along the $[00\bar{1}]_F$ direction have the complementary compositions $[U^4D_2F]$, $[D_4D_1U^1]$ and $[U^2D_3U^3]$ so that the composition of the ζ phase ($4D_j + 4U^i + F$) is both achieved and repeated every three columns along the $c_F$ direction.

The corresponding fluorite modular sequences for the known structures of ι-$M_7O_{12}$ and δ-$M_{11}O_{20}$ are given in Figs. 15(*b*) and 16(*b*) together with the c.d. diagrams from which these sequences were derived [Figs. 15(*a*) and 16(*a*)]. The $W_2^4$ fluorite module is found for the first time in the ι phase [Fig. 15(*b*)]. The sequences along the directions $[001]_F$ and $[100]_F$, namely

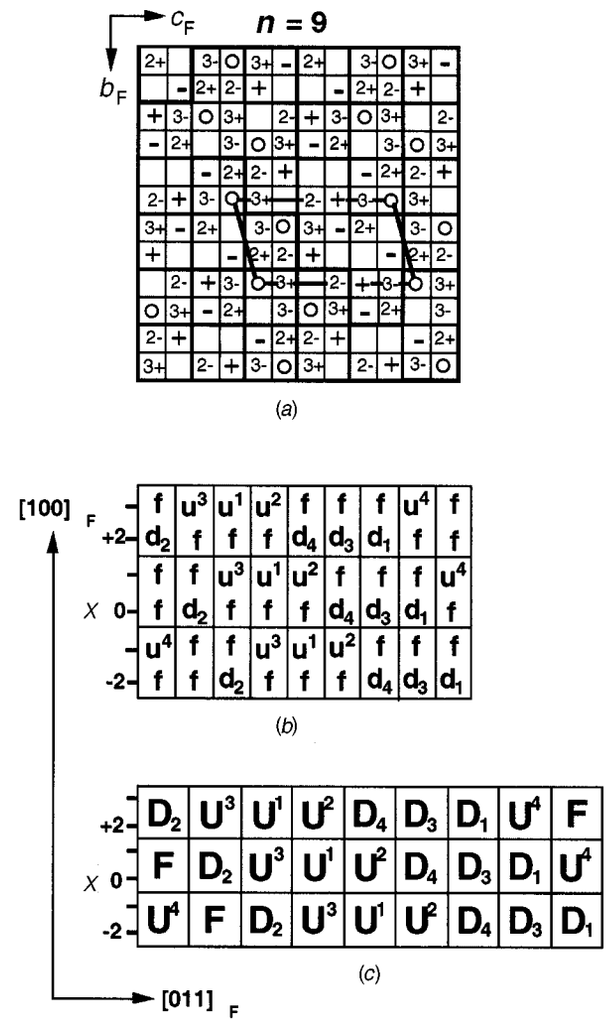


**Fig. 14** (*a*) The c.d. diagram for ζ-$M_9O_{16}$. (*b*) Fluorite hemicube modular sequences for $-2 \leqslant X \leqslant +3$. (*c*) Fluorite cube modular sequences along $[100]_F$ and $[011]_F$ directions

$[U^1D_1U^2W_2^4D_4U^3D_3]$ and $[U^1U^2D_4D_3D_1W_2^4U^3]$, unlike the ζ phase, are seen to be different [Fig. 15(*b*)]. From the c.d. diagram given in Fig. 15(*a*) the modular sequence along the $[010]_F$ direction, $[U^1D_4D_1U^3U^2D_3W_2^4]$, differs again from those given in Fig. 15(*b*). For the $n = 11$ phase the four $D_j$ and four $U^i$ modules are combined with three F modules to yield the required composition $M_{44}O_{80}\square_8$ of the δ phase. The fluorite modular sequences differ for each of the three principal axial directions, with the sequences along the $[010]_F$ direction, $[D_2FU^3D_3U^1D_1FU^4D_4FU^2]$, differing from those along the $[001]_F$ and $[100]_F$ directions, namely $[D_2D_1U^2U^1FD_3D_4U^3U^4FF]$ and $[D_2U^3U^1FD_4U^2D_3D_1U^4F]$, as listed in Fig. 16(*b*).

The modular sequences along the $[010]_F$ and $[00\bar{1}]_F$ directions for the ι-$M_7O_{12}$ and δ-$M_{11}O_{20}$ phases agree with those listed by Eyring and co-workers[6,14] provided that the c.d. diagrams are rotated through π/2 and the axial directions are redefined as above for the $n = 9$ phase.

The modular sequences for the unknown phase $M_8O_{14}$ are more complex but can be derived from the c.d. diagrams illustrated in Fig. 17(*a*) and (*c*) developed from the predicted monoclinic model represented in Fig. 9(*b*) and (*c*). For example, from the c.d. diagram 17(*a*) it is found that along the direction $[001]_F$ the sequence $[D_1U^4D_4U^3]_\infty$ at $X = 0$, 1+ is paired with either the sequence $[D_3U^1U^2D_2]_\infty$ or $[U^2D_2D_3U^1]_\infty$ occurring at $X = 2-/1-$ and $2+/3+$ respectively so that all eight $D_j$ and $U^i$ modules are employed in this bimodular alternation along the $a_F$ axis. However, it is evident from the c.d. diagram that the exact order of modules for each sequence is only repeated along the $[100]_F$ direction after every four modular layers. This arises

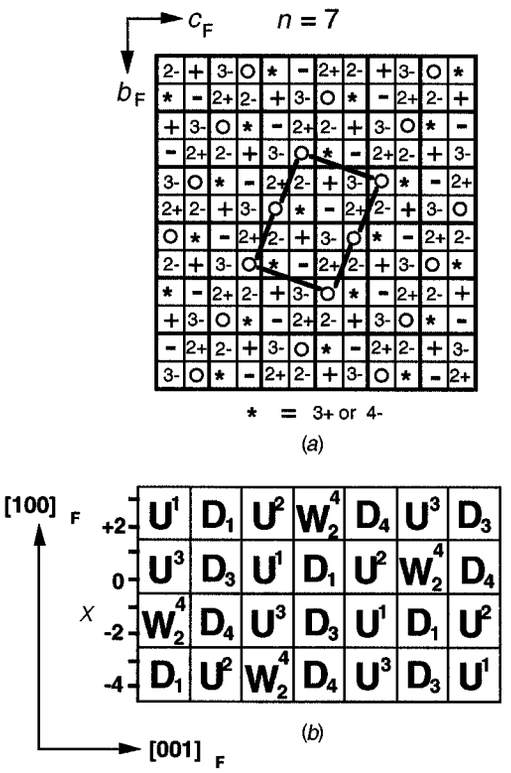


**Fig. 15** (*a*) The c.d. diagram for ι-$M_7O_{12}$. (*b*) Fluorite cube modular sequences along $[100]_F$ and $[001]_F$ directions for $-4 \leqslant X \leqslant +3$

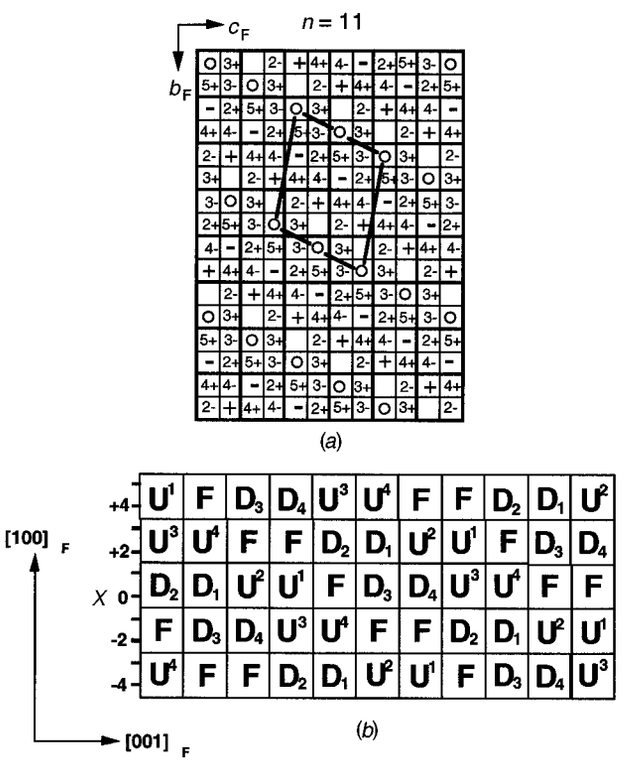


**Fig. 16** (*a*) The c.d. diagram for δ-$M_{11}O_{20}$. (*b*) Fluorite cube modular sequences along $[100]_F$ and $[001]_F$ directions for $-4 \leqslant X \leqslant +5$

because the individual A or B octant layers are only repeated up the $a_F$ axis for the values of $X = 0, 8, 16, \ldots$ *etc.* (see above). A similar pairing of modular quartets is also found along the $[010]_F$ and $[100]_F$ directions.

The fluorite modular sequences for the two triclinic $M_8O_{14}$ model structures proposed in Fig. 11(*b*) and 11(*c*) can be derived from the c.d. diagrams illustrated in Fig. 18(*a*) and 18(*b*). These are given in Fig. 18(*c*) and 18(*d*) from which it is

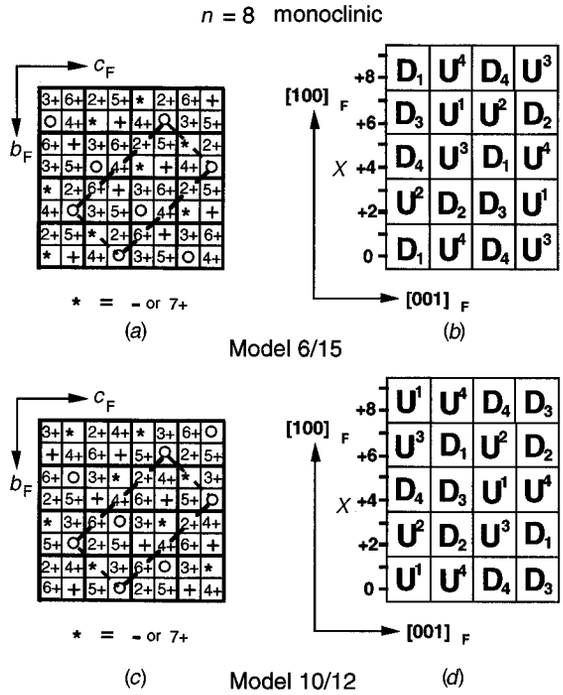


**Fig. 17** (*a*) and (*c*) The c.d. diagrams for the unknown $M_8O_{14}$ monoclinic phase. (*b*) and (*d*) Fluorite cube modular sequences along $[100]_F$ and $[001]_F$ directions $-1 \leqslant X \leqslant +7$

seen that for model 7/12 the sequence $[D_4U^3D_1U^2D_2D_3U^1U^4]$ along the direction $[001]_F$ or $[0\bar{1}0]_F$ differs from that $[D_4D_3D_1U^4D_2U^3U^1U^2]$ along the $a_F$ axis. Similarly, for model 5/14, the sequence $[D_4D_3U^1U^2D_2U^3D_1U^4]$ along the direction $[001]_F$ or $[0\bar{1}0]_F$ differs from that $[D_4U^3U^1U^4D_2D_3D_1U^2]$ along the $a_F$ axis. It is quite clear, therefore, that contrary to Eyring and co-workers,[6,14] the eight basic fluorite modules can share faces to generate two model triclinic structures of composition $M_{32}O_{56}\square_8$ in three dimensions.

## Conclusion

It has been demonstrated that the co-ordination defect theory applied to defect fluorite-related lanthanoid oxides is not only a powerful method for predicting model structures for both known and unknown ordered phases including polymorphs, but also for determining modular sequences. The generation of c.d. diagrams which provide a detailed map of the exact location of vacant anion sites in successive $\{100\}_F$ layers of the model structure depends on employing the fluorite octant as the primary structural module from which both the co-ordination defect and the predicted structures are assembled. Recognition of the left- and right-handedness of both the octants and therefore of the c.d., together with the unique topology of the latter, are crucial elements leading to the prediction of unknown structures and their modular sequences.

The predictive value of the F, $D_j$, $U^i$ and $W_j^i$ module set has serious limitations because Eyring and co-workers[6,14] have not recognized adequately the fundamental importance of the integrity and topology of the co-ordination defect in defect fluorite-related systems. This is demonstrated by their inability to devise a model for the unknown phase of composition $M_8O_{14}$. They have also attempted[6] to model much larger compounds such as $Ce_{19}O_{34}$ for which the structure is also unknown. For this oxide they have proposed a module sequence which contains both divacancy pairs and single vacancy pairs in equal numbers and therefore unexpectedly incorporates a $W_j^i$ module. In marked contrast, application of the c.d. theory to this compound[16] reveals that there are actually six, not one, permitted modular sequences all of which are consistent with the triclinic symmetry and unit-cell parameters reported[19] for

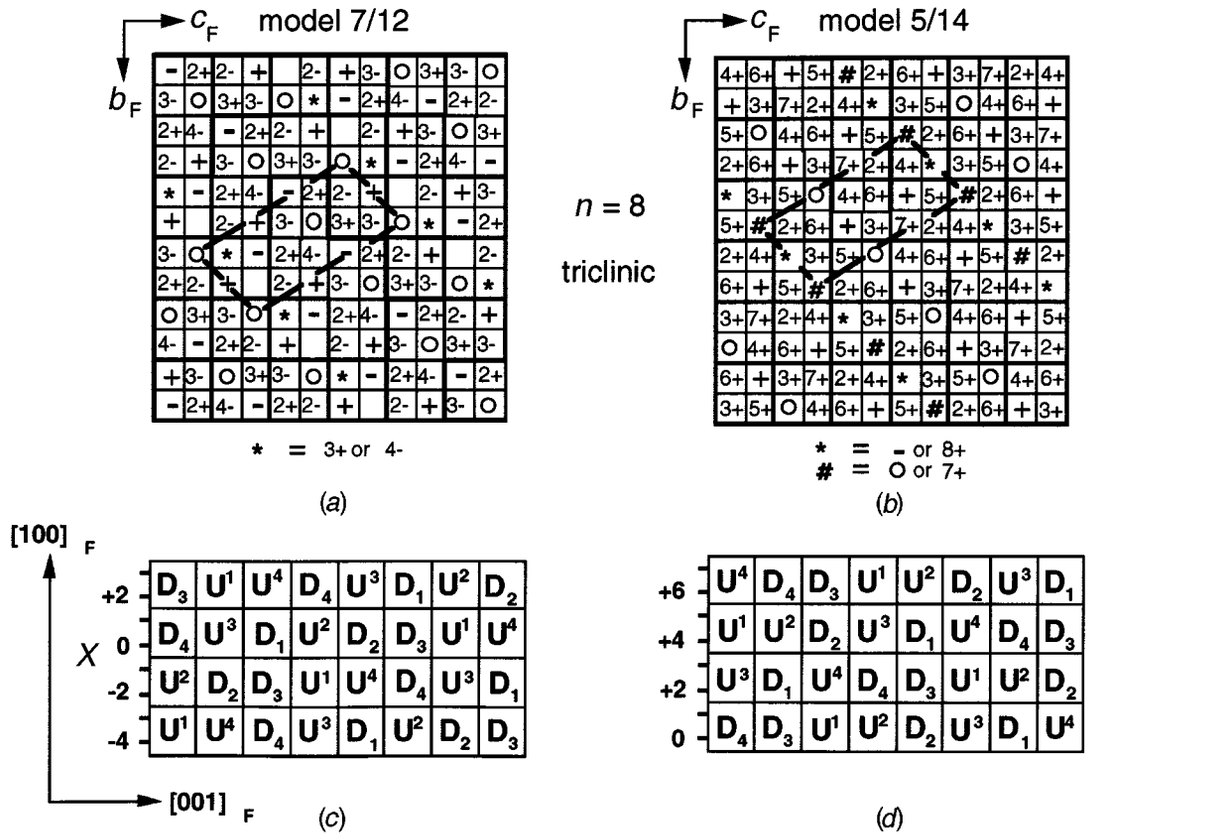


**Fig. 18** The c.d. diagrams for the unknown $M_8O_{14}$ triclinic phase: (*a*) model 7/12, (*b*) 5/14. Fluorite cube modular sequences along $[100]_F$ and $[001]_F$: (*c*) model 7/12 for $-4 \leqslant X \leqslant +3$, (*d*) model 5/14 for $-1 \leqslant X \leqslant +6$

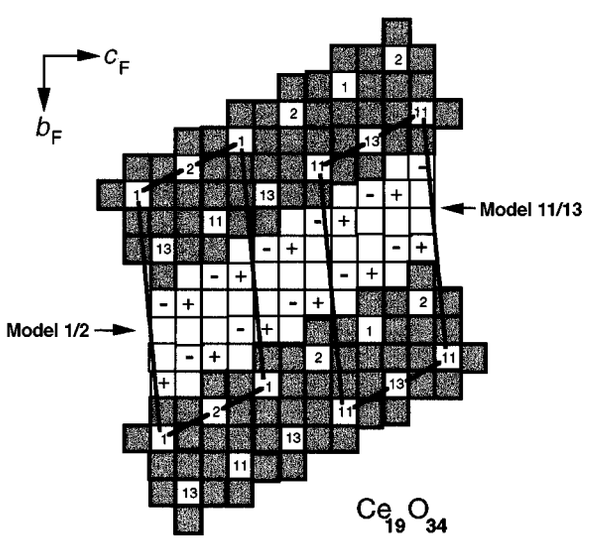


**Fig. 19** One predicted model for the $Ce_{19}O_{34}$ triclinic phase. Structural repeat unit in the $(100)_F$ layer outlined for models 11/13 and 1/2

$Ce_{19}O_{34}$. For example, one of the remaining five structures predicted for $Ce_{19}O_{34}$ is illustrated for a $(100)_F$ layer in Fig. 19 with the modular sequence $[D_4D_3FD_1D_2U^4U^3FU^1U^2D_1D_2D_4D_3FU^1U^2U^4U^3]$ along the $[001]_F$ direction.[16] Interestingly, all five of the predicted sequences involve the unit-cell content $(3F8U^i8D_j)$ whereas only the sixth sequence, formulated by Kang and Eyring[6] as $(4FW_j^i7U^i7D_j)$, involves a $W_j^i$ module (although this module was overlooked[6] for $Ce_{19}O_{34}$ in their Table 2). Although these authors recognized that the incorporation of a $W_j^i$ module was unlikely for a phase with such a large value of *n*, their failure to predict any one of the five remaining possible and more satisfying models led them to suggest that $Ce_{19}O_{34}$ must be an unusual 'transitional phase'. Not surprisingly, Kang and Eyring[6] were forced to admit that the selection and orientation of modules to achieve an appropriate fluorite modular sequence in their hands is 'a trial and error process guided by experience, a perception of thermodynamic considerations, and the emerging order in the growing sequence'.[6]

Finally, attention is drawn to the fact that if either of the hemicubes $d_j$ or $u^i$ of composition $M_2O_3\square$ were combined with four fluorite octants of individual composition $M_2O$, it would be possible to construct a new module of composition $M_4O_7\square$ which would possess the marked advantage of incorporating the structure-determining topology of the co-ordination defect. This can be achieved by placing each of the four additional octants in juxtaposition with the untenanted oxygen site of the parent $d_j$ or $u^i$ hemicubes. The resulting new molecules are illustrated in Fig. 20 and are designated here as $L_j$ and $H^i$ modules. If no anion vacancy were present, the eight octants would be compositionally equivalent to the fluorite module F. These new modules conform to the rules set out and can readily be identified in the c.d. patterns reproduced in Figs. 14–18. Thus, for example, the modular sequence for $\zeta$-$M_9O_{16}$ along the $[011]_F$ direction would become $[FL_2H^3H^1H^2L_4L_3L_1H^4]$ with the required composition $M_{36}O_{64}\square_8$; the sequences for some of the other oxides are listed in Table 1.

Fig. 21 illustrates how the combination of an $H^4$ with a $L_2$ module generates a new module of composition $M_8O_{14}\square_2$ containing two vacancies and termed here a $Z_j^i$ module. If the two fluorite octants (marked with an H in Fig. 21) were eliminated, a comparison with Fig. 5(*B*)(*d*) would reveal that the resulting module which remains is actually a c.d. pair sharing six faces along the $[111]_F$ direction with the composition $M_7O_{12}\square_2$. Alternatively, the $Z_j^i$ module may be viewed as Eyring's $W_j^i$ module of composition $M_4O_6\square_2$ which is featureless in topological terms [Fig. 13(*e*)], to which eight peripheral fluorite octants have been added to incorporate the structure-determining topology of the c.d.

The topological advantages for structure prediction of the $L_j$, $H^i$ and $Z_j^i$ modules over Eyring's $D_j$, $U^i$ and $W_j^i$ fluorite cubes,

**Table 2** Some defect fluorite-related modules

| Module | Composition | Phase | Topology | Icon * |
|---|---|---|---|---|
| Octant | $M_2^iO$ | δ or λ | Inactive | o |
| | $M_2^i\square$ | δ or λ | Inactive | $o^0$, $o^+$, $o^-$, *etc.* |
| Quadrant | $MO_2$ | δλ or λδ | Inactive | $f_j^i$ |
| (along | $MO\square$ | δλ or λδ | Inactive | $q^i$ or $q_j$ |
| $\frac{1}{2}\langle 111\rangle_F$) | $M\square_2$ | δλ or λδ | Inactive | $w_j^i$ |
| Hemicube | $M_2O_4$ | 2δ + 2λ | Inactive | f |
| | $M_2O_3\square$ | 2δ + 2λ | Inactive | $u^i$ or $d_j$ |
| Co-ordination defect | $M_{3.5}O_6\square$ | δ + 6λ or λ + 6δ | Active | c.d. |
| | $M_7O_{12}\square_2$ | 7δ + 7λ | Active | $(c.d.)_2$ |
| Cube | $M_4O_8$ | 4δ + 4λ | Inactive | F |
| | $M_4O_7\square$ | 4δ + 4λ | Inactive | $U^i$ or $D_j$ |
| | $M_4O_6\square_2$ | 4δ + 4λ | Inactive | $W_j^i$ |
| Topotactic | $M_4O_8$ | 6δ + 2λ or 2δ + 6λ | Active | F |
| | $M_4O_7\square$ | | Active | $H^i$ or $L_j$ |
| | $M_8O_{14}\square_2$ | 8δ + 8λ | Active | $Z_j^i$ |

* $i = 1$–4, $j = 1$–4; $(i,j) = (1, 3), (2, 4), (3, 1), (4, 2)$.

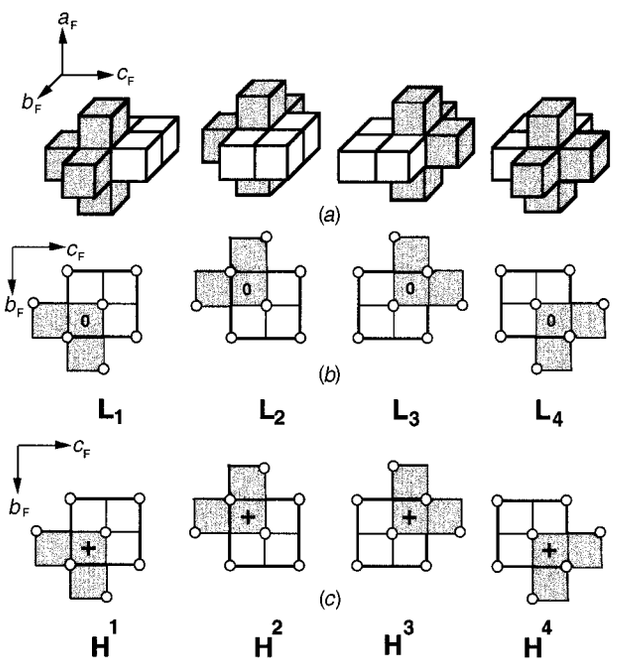


**Fig. 20** Representations of eight (with composition $M_4O_7\square$) of the thirteen topotactic modules from which all the binary lanthanoid oxides can be modelled. (*a*) Three-dimensional representation showing the topology of four possible topotactic modules. (*b*) Matrix representation of four possible topotactic modules, $L_j$ in the $X = 0$ layer. (*c*) Four possible topotactic $H^i$ modules in the $X = 1$ layer

all of which are featureless in topological terms, will be evident. Nevertheless, having predicted all the possible model structures for a fluorite-related oxide from its c.d. diagram, there remains some value in being able to provide an alternative modular representation of the resulting structures in terms of a modular sequence because each structure can then be expressed by a row of icons in any defined direction. Some of the many icons that can be employed for this purpose have been outlined in this paper and are summarized in Table 2.

Catlow and co-workers[20] have recently carried out substantial computer-simulation studies of defect fluorite lattices and, in particular, have calculated the energies of defect formation at the $(110)_F$ and $(111)_F$ surfaces of $CeO_2$ using atomistic simulation techniques based on the Born model of the ionic solid.

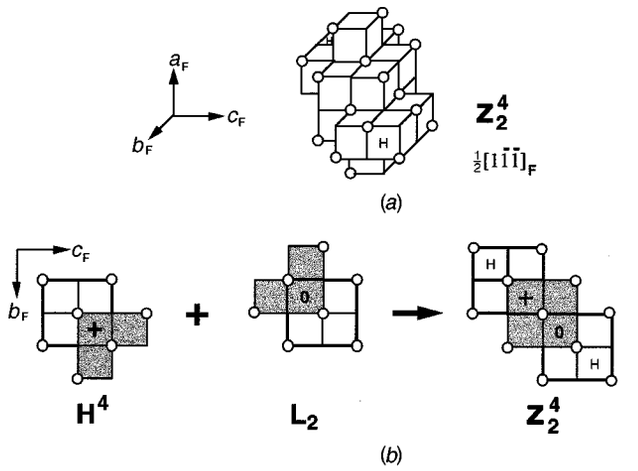


**Fig. 21** (*a*) Three-dimensional representation of a topotactic $Z_j^i$ module of composition $M_8O_{14}\square_2$. (*b*) Topotactic $Z_j^i$ module formed by overlaying a $L_2$ module in a $X = 0$ layer with a $H^4$ module in the $X = 1$ layer

Unlike the co-ordination defect, a surface vacant oxygen site will be co-ordinatively unsaturated so that it is difficult to compare the present treatment with the results obtained from computer modelling. However, it would be interesting to evaluate whether a simulation model based on c.d. clusters embedded in the fluorite matrix would predict the existence of the observed homologous series, $M_nO_{2n-2m}$.

## Acknowledgements

Stimulating discussions with Dr. B. F. Hoskins and Professor D. J. M. Bevan are gratefully acknowledged.

## References

1 Part 5, B. F. Hoskins and R. L. Martin, *Aust. J. Chem.*, 1995, **48**, 709.
2 R. L. Martin, M.Sc. Thesis, University of Melbourne, 1948.
3 R. L. Martin, *Nature* (*London*), 1950, **165**, 202.
4 M. R. Thornber, D. J. M. Bevan and J. Graham, *Acta Crystallogr., Sect. B*, 1968, **24**, 1183.
5 R. L. Martin, *J. Chem. Soc., Dalton Trans.*, 1974, 1335.
6 Z. C. Kang and L. Eyring, *Aust. J. Chem.*, 1997, **49**, 981.
7 L. Eyring and Z. C. Kang, *Eur. J. Solid State Chem.*, 1994, **31**, 717.
8 P. Kunzmann and L. Eyring, *J. Solid State Chem.*, 1975, **14**, 229.
9 B. F. Hoskins and R. L. Martin, *J. Chem. Soc., Dalton Trans.*, 1976, 676.
10 J. Zhang, Z. C. Kang and L. Eyring, *J. Alloys Compd.*, 1993, **192**, 57.
11 J. Zhang, R. B. Von Dreele and L. Eyring, *J. Solid State Chem.*, 1993, **104**, 21.
12 J. Zhang, R. B. Von Dreele and L. Eyring, *J. Solid State Chem.*, 1995, **118**, 133 and 141.
13 J. Zhang, R. B. Von Dreele and L. Eyring, *J. Solid State Chem.*, 1996, **122**, 53.
14 Z. C. Kang, J. Zhang and L. Eyring, *Z. Anorg. Allg. Chem.*, 1996, **622**, 465.
15 R. B. Von Dreele, L. Eyring, A. L. Bowman and J. L. Yarnell, *Acta Crystallogr., Sect. B*, 1975, **31**, 971.
16 R. L. Martin, unpublished work.
17 B. G. Hyde, D. J. M. Bevan and L. Eyring, *Philos. Trans. R. Soc. London, Ser. A*, 1966, **259**, 583.
18 R. L. Martin, *Proc. R. Soc. N.S.W.*, 1976, **109**, 137.
19 P. Knappe and L. Eyring, *J. Solid State Chem.*, 1985, **58**, 312.
20 T. Sayle, S. C. Parker and C. R. A. Catlow, *J. Chem. Soc., Chem. Commun.*, 1992, 977.

*Received* 8*th July* 1997; *Paper* 7/04836J